



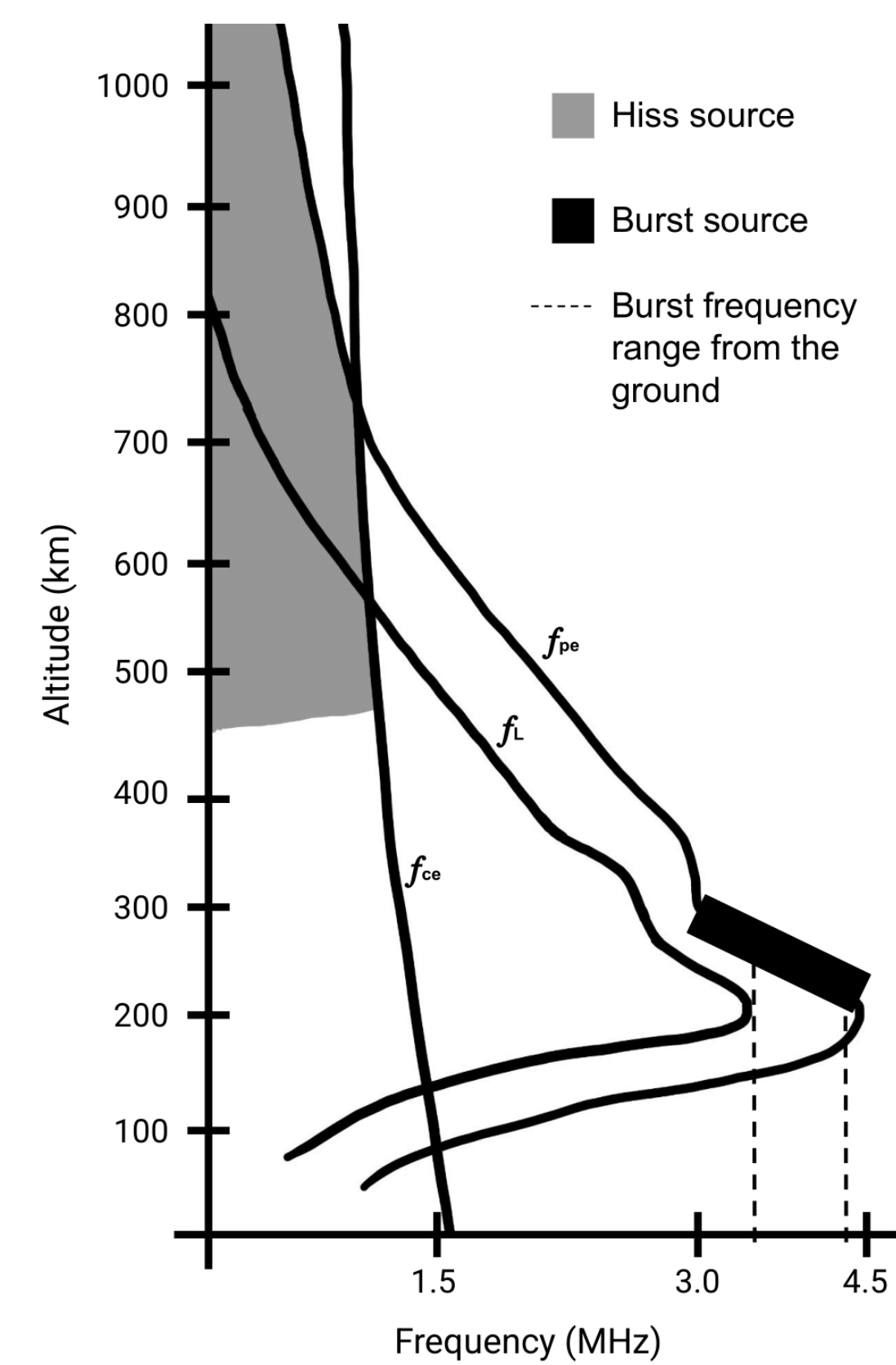
Direction Finding of Simultaneous Medium Frequency Burst and Hiss Auroral Radio Emissions

T. M. Godfrey, J. LaBelle

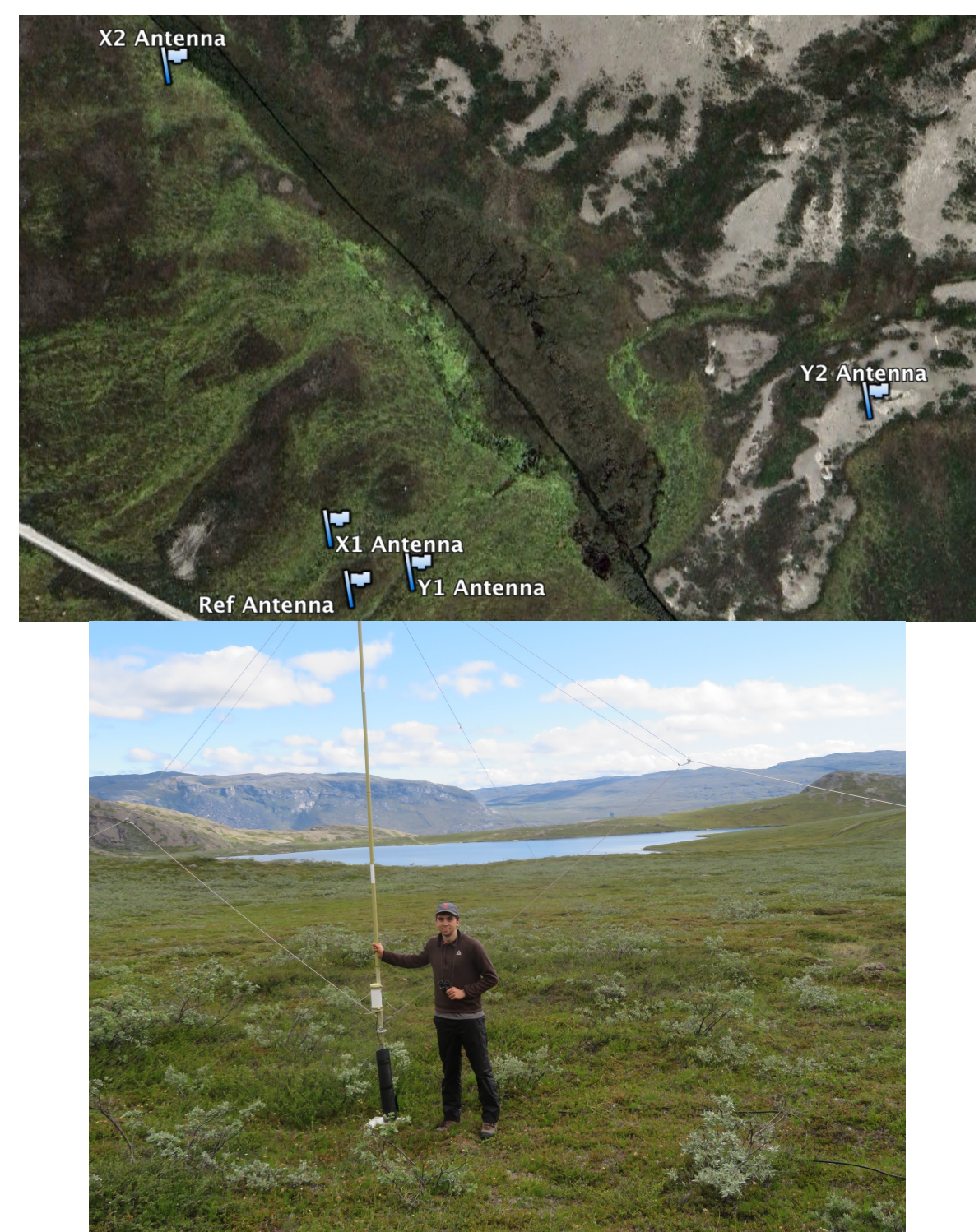
Dartmouth College, Department of Physics and Astronomy

Introduction

This study uses direction finding to establish the DOA for simultaneously occurring auroral hiss and medium frequency burst (MFB), and to determine if these events could come from the same auroral electron beam. Auroral hiss is a VLF/LF whistler-mode emission originating at altitudes of several hundred to several thousand kilometers. MFB spans 1.5–4.5 MHz and is suspected to originate in the ionospheric topside. These emissions often coincide in time, but it is unknown the degree to which they are spatially correlated. This question will be addressed using data collected over two years (2015–2017). Data were collected with a five-antenna array (pictured in the images below) in Sondrestrom, Greenland (73.3° magnetic latitude). The larger array was used for the higher frequency channels (850–3100 kHz) where MFB is observed. The smaller array was used for the 100–850 kHz frequency range where auroral hiss is observed, and both arrays share the reference antenna shown.



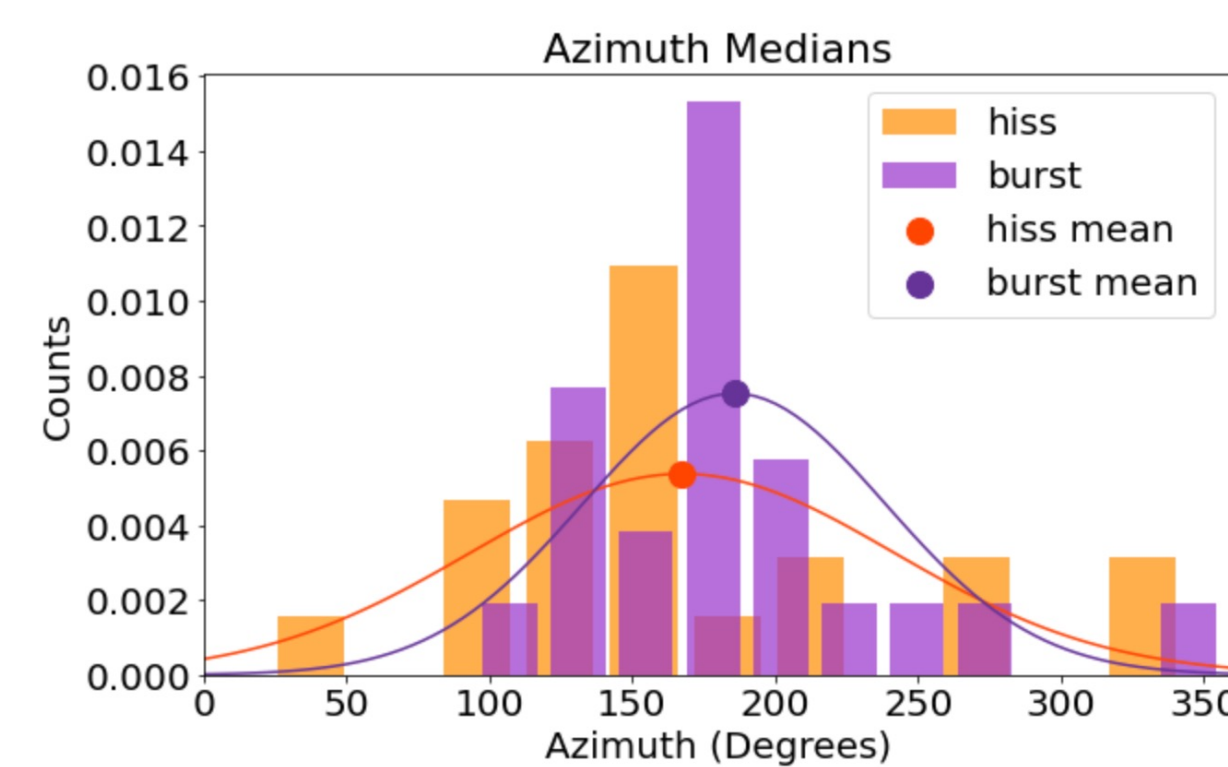
The figure above shows frequency as a function of altitude and is an illustration of the criteria for MFB and hiss. It shows one of the potential topside generation mechanisms for MFB that allows for a range of frequencies in which Langmuir waves on the topside of the ionosphere can convert to L-mode waves and can reach ground-level if their frequency exceeds the maximum L-cutoff frequency in the ionosphere. (Broughton et al., 2012) The black bar along the f_{pe} profile indicates the region where the MFB can be generated. The MFB is only able to reach ground-based antennas at frequencies above the f_L profile. The greyed region indicates the region below f_{pe} and f_{ce} , where the auroral hiss can be generated at notably higher altitudes than the MFB.



Results

A total of forty simultaneous MFB and hiss auroral emissions were observed over the two-year period. Of these, eighteen were discarded due to the power being too low or due to one of the channels not collecting data. For each of the twenty-two good events remaining, the analysis described in the methodology was done. The resulting median and corresponding MAD values found for both azimuth and elevation were statistically analyzed separately using four Boolean criteria:

- 1) MFB and hiss medians within one MAD
2) MFB or hiss medians within one MAD
3) Any overlap of MFB and hiss MAD
4) No overlap of MFB and hiss MAD



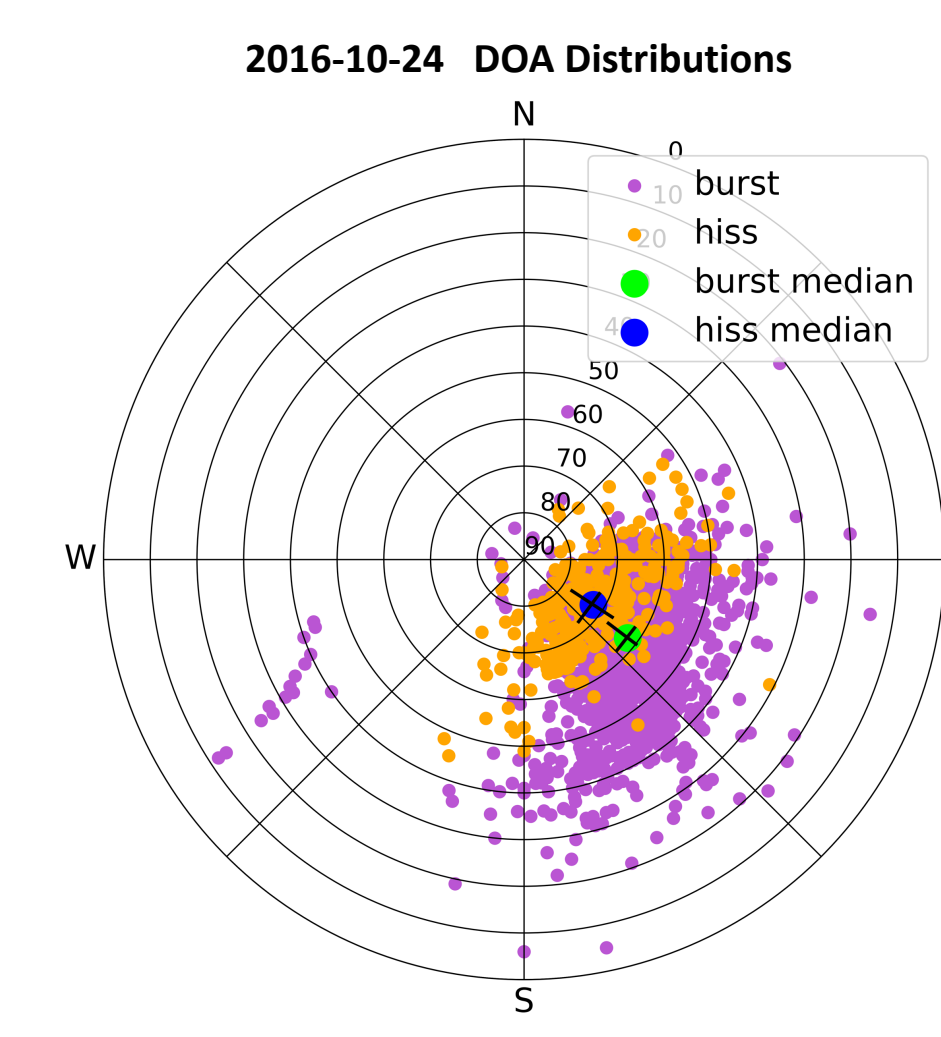
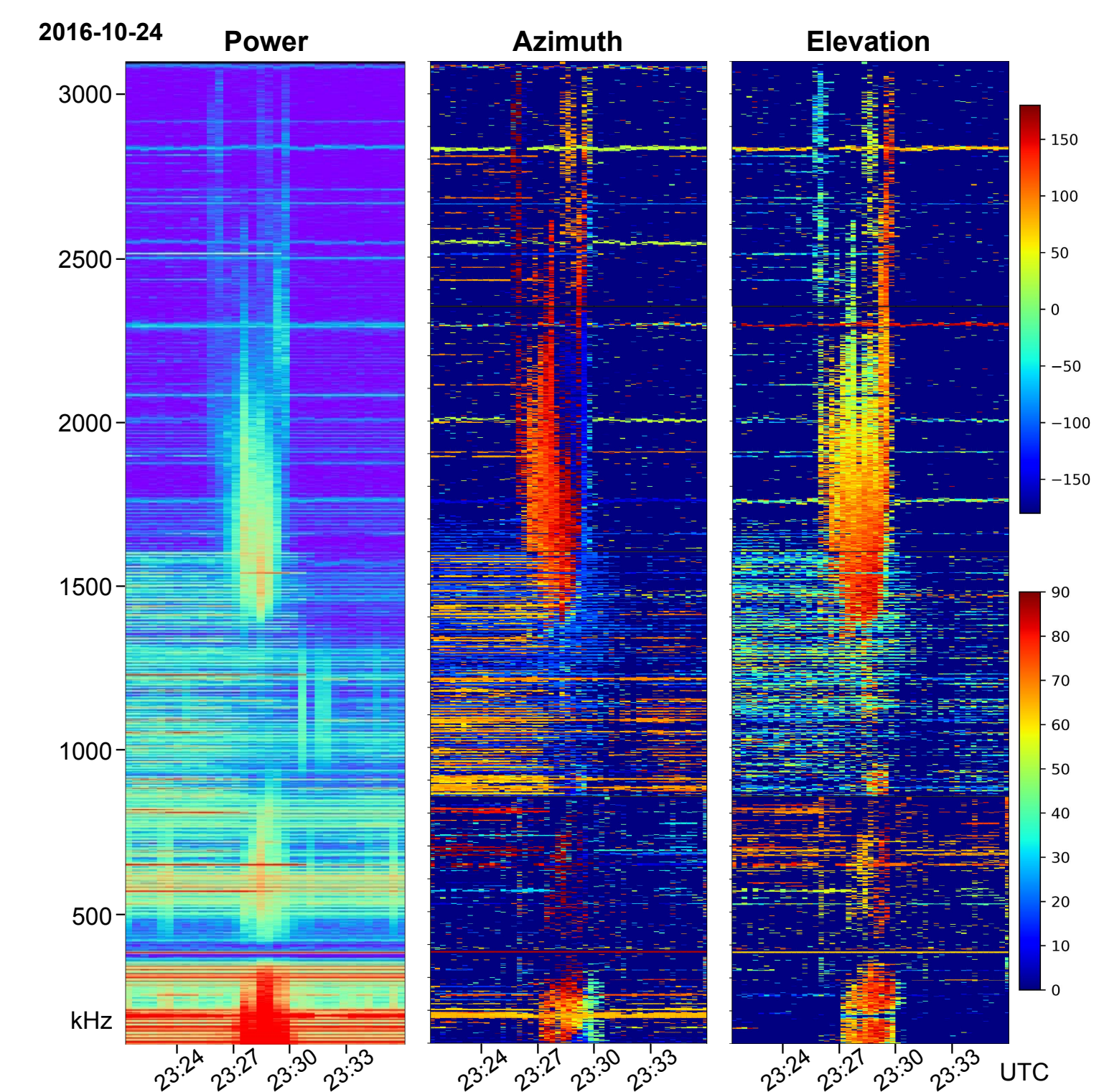
From the twenty-two azimuth and elevation median values the mean, variance, and standard deviation was determined as shown in the histograms to the right. The upper histogram shows the azimuth medians in which the hiss is shown in orange, and the burst is shown in purple. The corresponding mean for the hiss and burst is also shown in red at 167.41° and violet at 185.53°, respectively. The lower histogram shows the elevation medians in which the hiss is shown in light blue at 80.27°, and the MFB is shown in grey at 64.88°.

The corresponding mean for the hiss and burst is also shown in dark blue and black, respectively. A truncated Gaussian was fit to each of the distributions. The difference in the azimuth means was found to be 18.12° out of 360° or 5.03% and the difference in the elevation means was found to be 15.39° out of 90° or 17.1%. The larger percent difference in the elevation medians is expected and is due to the hiss sourcing from a higher altitude than MFB.

For the MFB and hiss azimuth values, the Boolean analysis resulted in: 1) 2/22 or 9.09%, 2) 16/22 or 72.73%, 3) 18/22 or 81.82%, 4) 4/22 or 18.18%. These results were not unexpected for events that have similar azimuth values, as the strictest criteria (1 and 4) had the least amount of truth-value, and the least strict (2 and 3) had the most truth-value. The hiss MAD was more typically the reason for the overlap, since it often covered a broader range of azimuth values by being at higher elevations close to 90°.

For the MFB and hiss elevation values, the Boolean analysis resulted in: 1) 1/22 or 4.55%, 2) 3/22 or 13.64%, 3) 7/22 or 31.82%, 4) 15/22 or 68.18%. Again, these results were not unexpected for events that have largely differing elevation values. This difference in elevation values is expected since hiss likely sources from higher altitudes in the ionosphere.

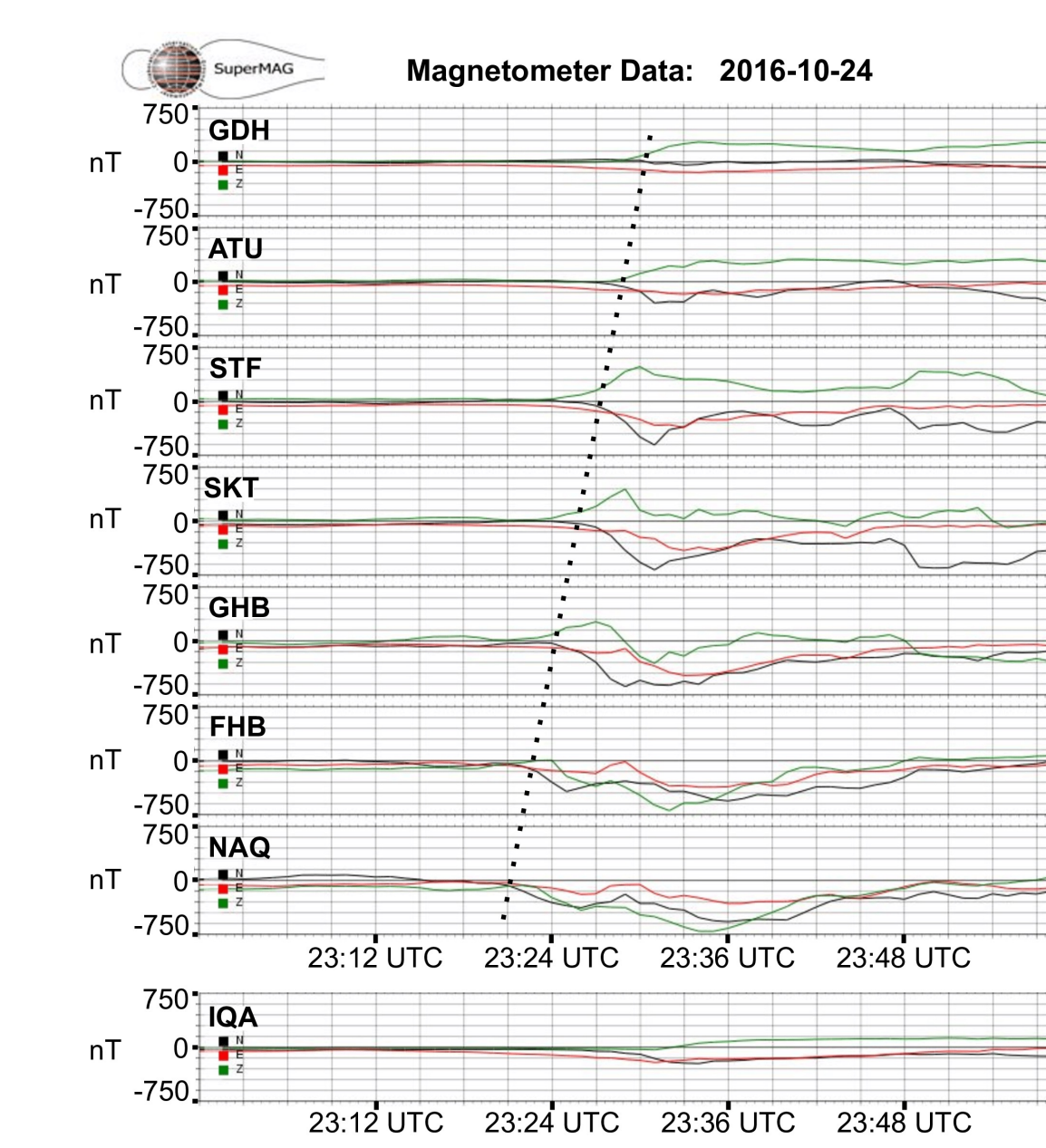
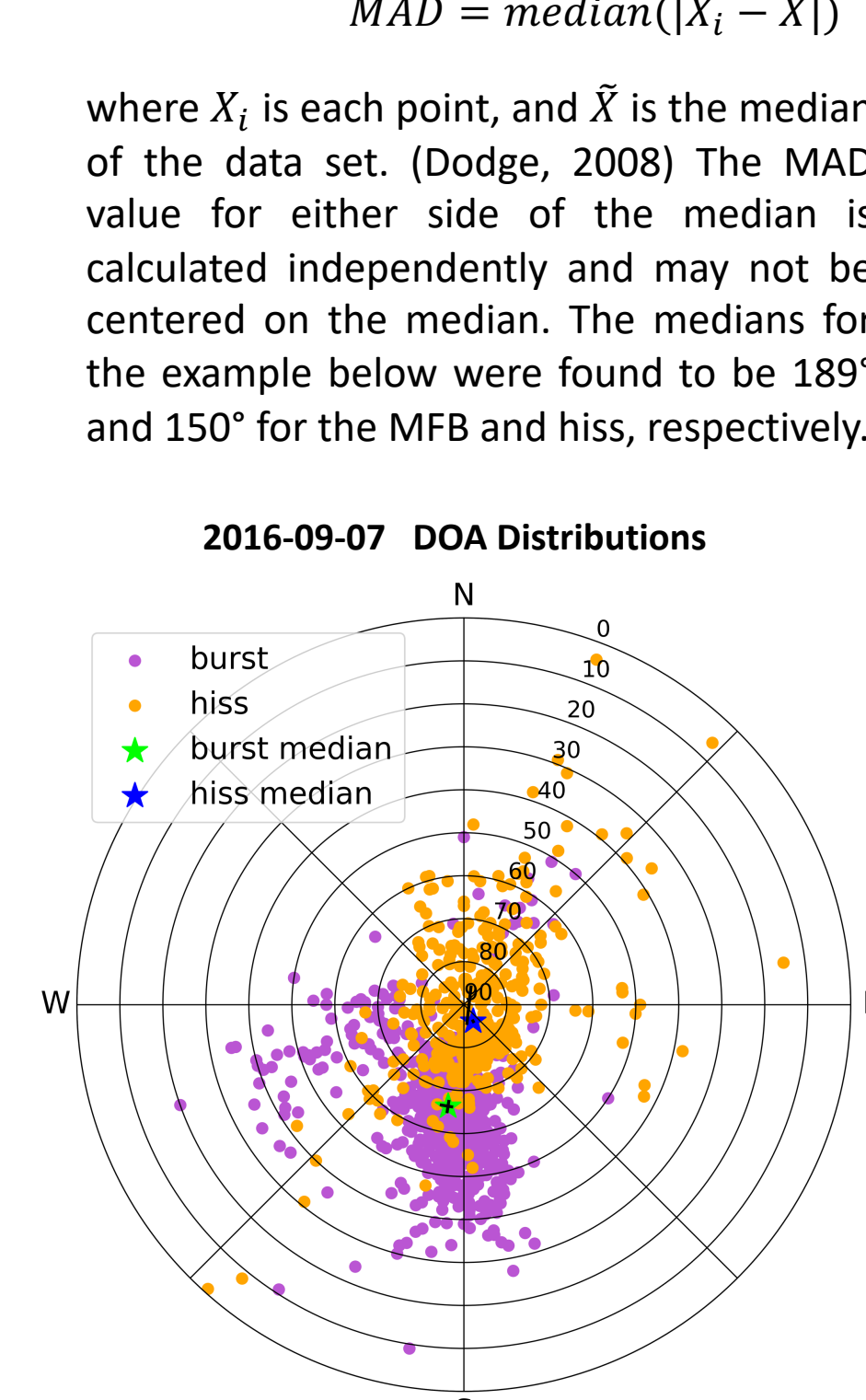
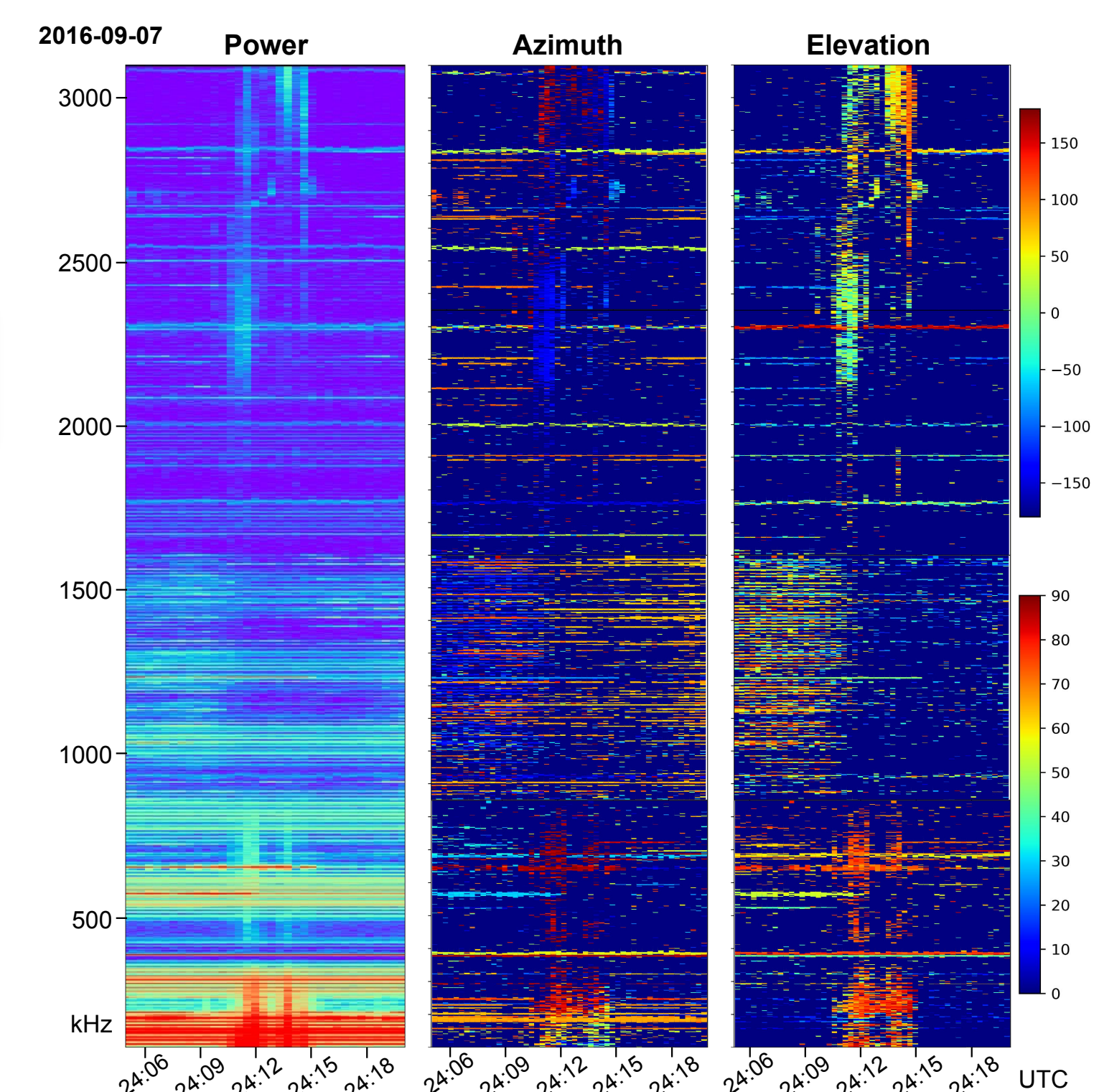
Methodology



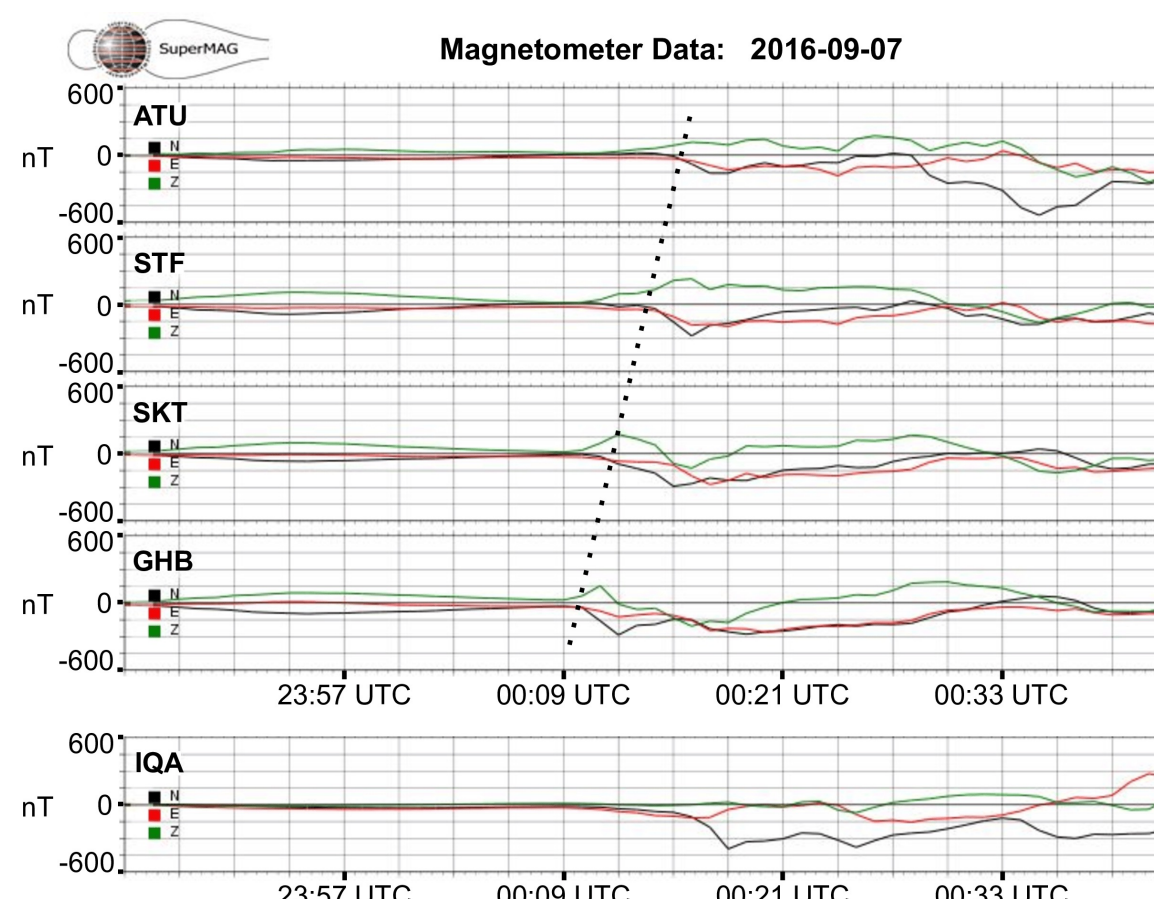
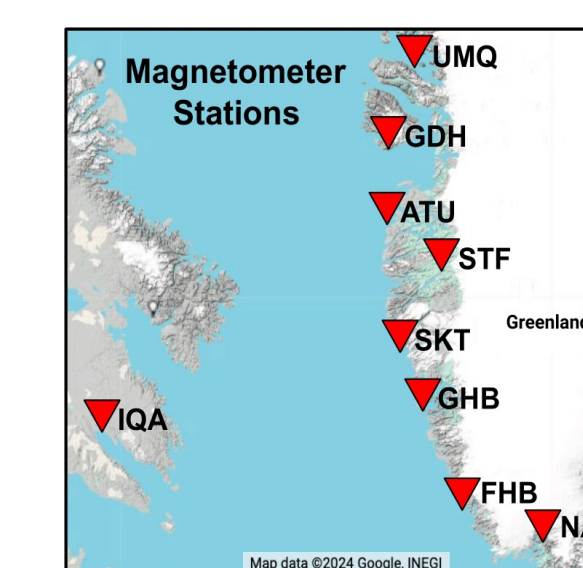
A click and drag box selection tool (not shown) was developed in python to analyze auroral events from spectrograms. It also allows for the removal of interference lines and filtering by power and frequency. Here, the radial component represents the elevation angle of arrival, and the angular component represents the azimuthal angle of arrival. The medium frequency burst is shown in purple, and the hiss is shown in orange. The median values of the were used rather than mean values for analysis to minimize the effect of outliers and scatter in the distributions. The medians are shown in green and blue for the MFB and hiss, respectively, and were found to be 127° and 123° in the above example. The median absolute deviation (MAD) in elevation and azimuth for each auroral event type is given by the error bars, and is defined as

MAD = median(|Xi - X|)

where Xi is each point, and X is the median of the data set. (Dodge, 2008) The MAD value for either side of the median is calculated independently and may not be centered on the median. The medians for the example below were found to be 189° and 150° for the MFB and hiss, respectively.



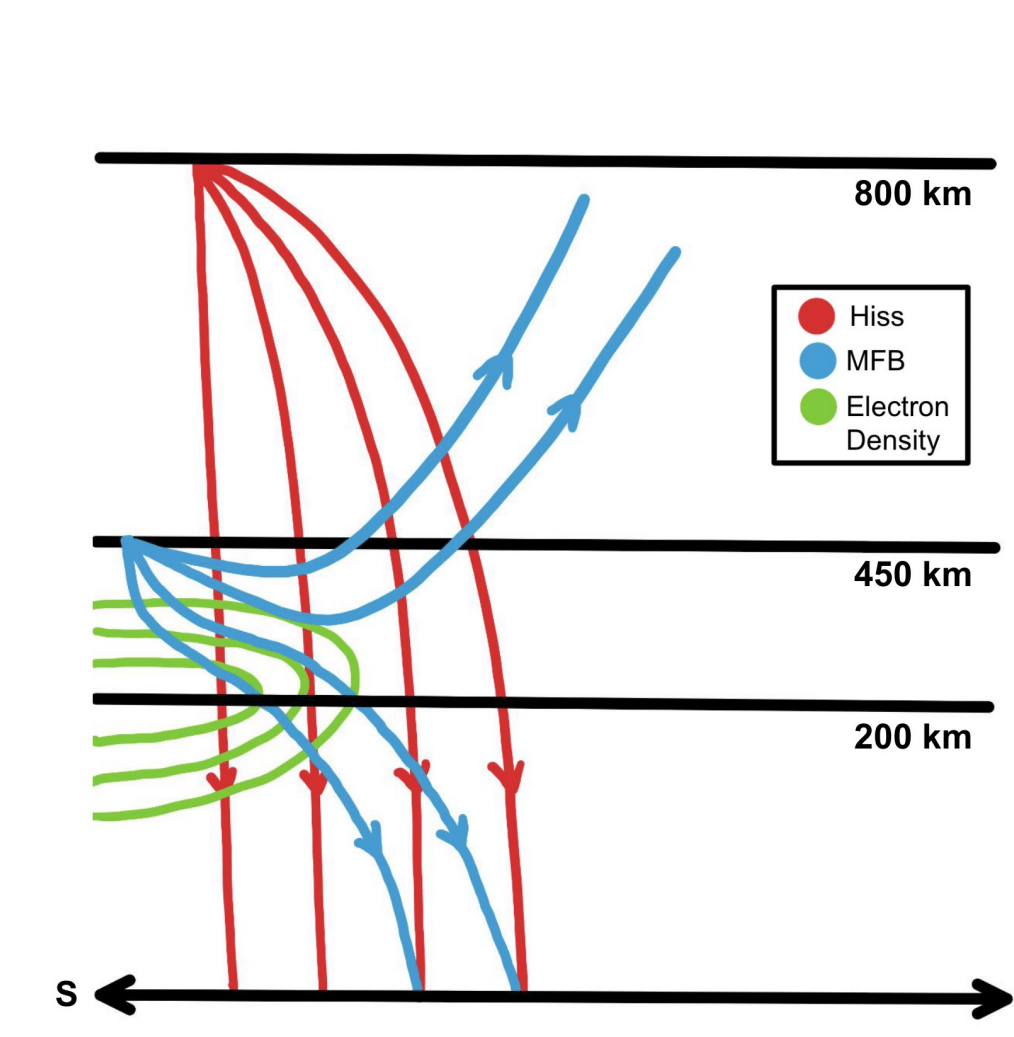
Magnetometer data for both simultaneous hiss and MFB event examples is shown above and below was retrieved from SuperMAG (Gjerloev et al., 2012) using several Eastern Greenland and Western Canadian stations displayed geographically in the map below, where STF is Sondrestrom. A one-hour interval centered on the start time of the simultaneous event observed at Sondrestrom are shown in order from North to South (top to bottom). The dotted line superposed is meant to approximate the cardinal movement in direction of the initial substorm observation and does not account for the East/West movement which can be seen in the spectrograms to the left. The magnetometer data in both examples shown indicates that the auroral substorms started at a lower geographic latitude than Sondrestrom and then moved Northward above the station.



Discussion

The figure to the right shows the expected behavior of the auroral hiss (red) and MFB (blue) in an arbitrary electron density contour (green). The auroral hiss is theoretically generated at significantly higher altitudes than MFB. As shown by the figure, the hiss starts at 800 km and the MFB starts at 450 km, both of which are initially above the electron density contour. This difference in initial altitude is due to the generation mechanism conditions given in the introduction, and the propagation will follow magnetic field lines closely. As mentioned in the ray tracing section, the Whistler mode wants to be parallel to the magnetic field lines, so future work will include using a VLF ray tracing software or the 3D version of PHARLAP.

When an auroral electron beam is formed some of the electrons are faster than others and rush ahead over some distance. This leads to the formation of an unstable distribution and generates waves. The generation of these waves causes the electrons to lose energy and fill the distribution back in, as shown in the second figure to the right from an electron beam study from a broader context of solar radio emissions and interplanetary



plasma. (Muscietti, 1990) This re-absorption can repeat many times as the electrons stream through the plasma in the ionosphere and depends primarily on the starting altitude and the strength of the electron density.

In summary, this study looks to estimate a range of initial altitudes for both MFB and hiss, by using the measured elevation and azimuth DOA for the MFB and hiss ray traces in combination with an electron density model from Sondrestrom ISR data. The initial altitudes of interest are where the MFB and hiss rays reach approximately the same ground range. From these values a model of the auroral electron beam evolution between the initial heights can be created to establish if it is plausible for the same auroral electron beam to cause both emissions by the beam reformation process described.

Ray Tracing

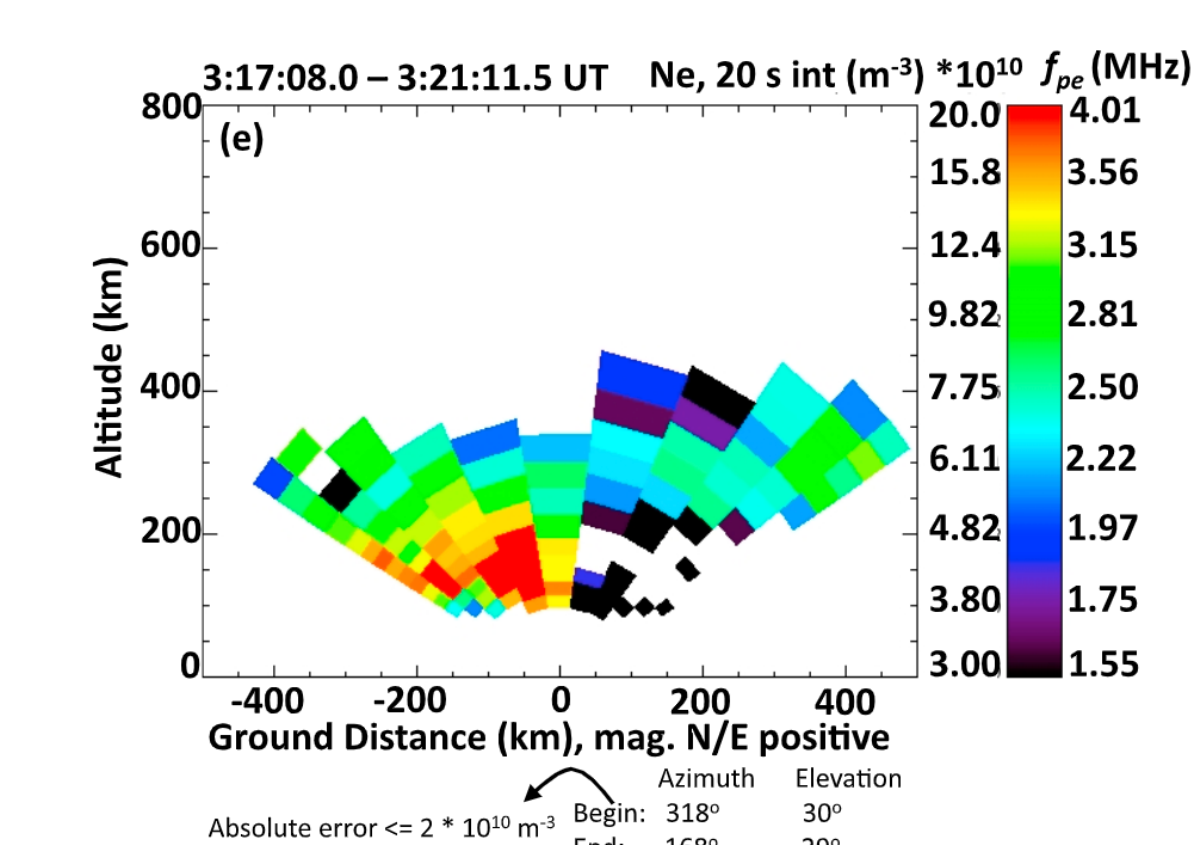
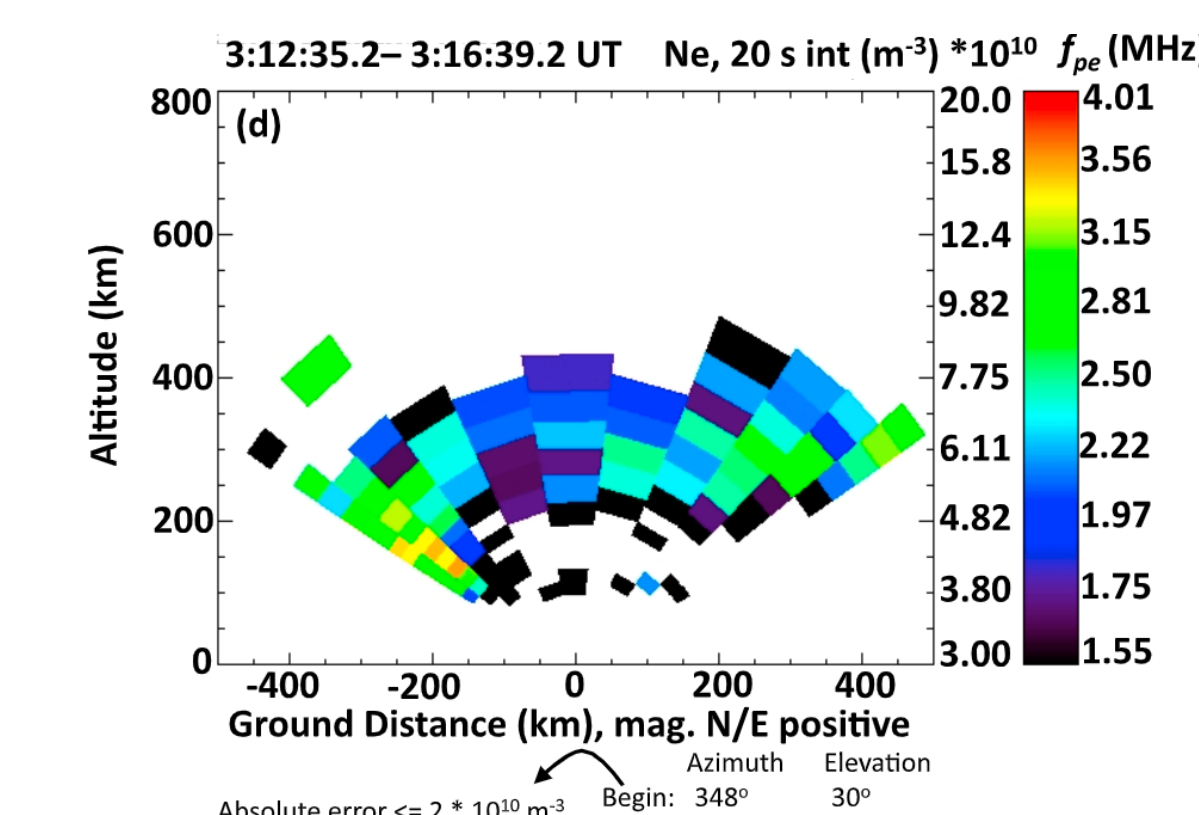
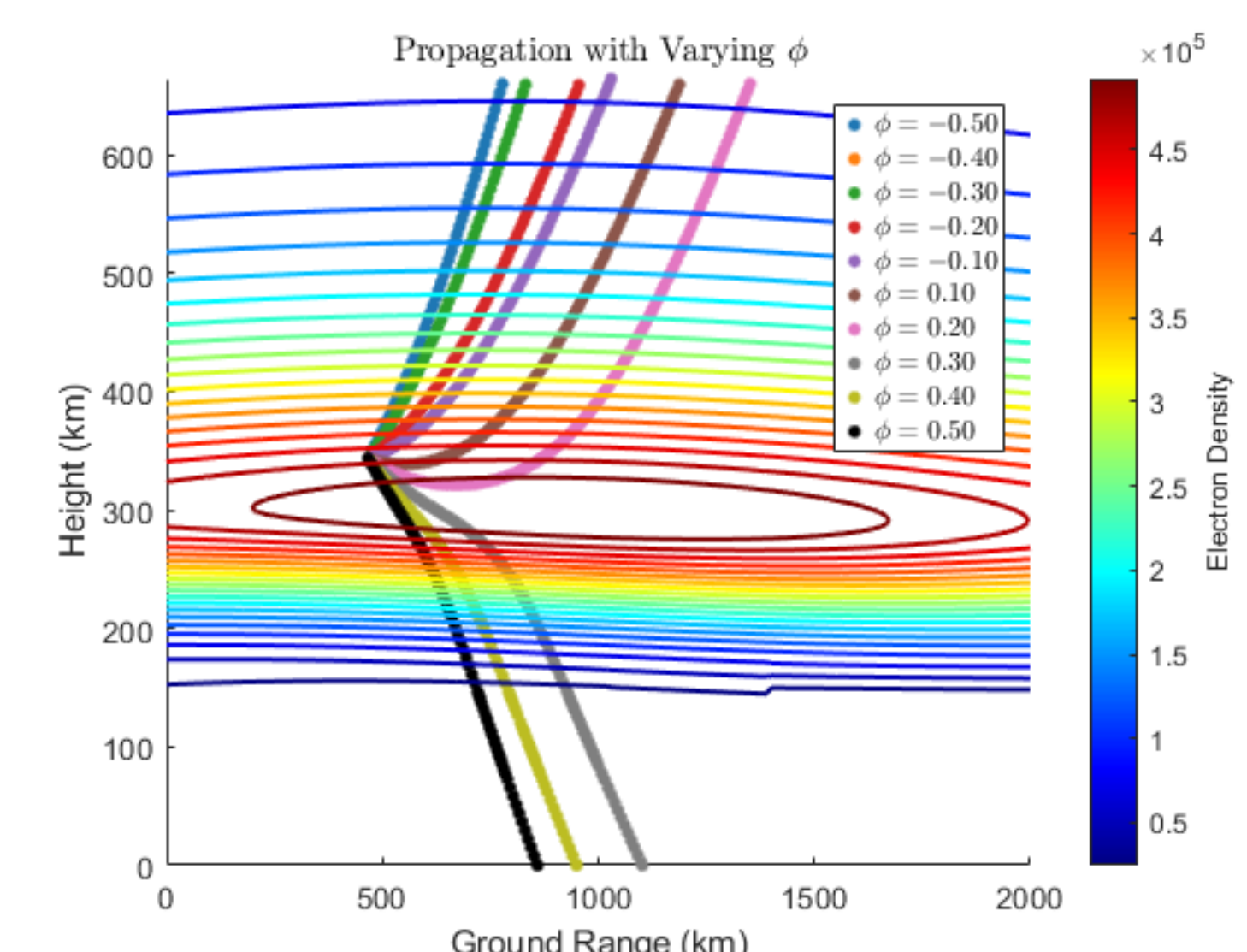
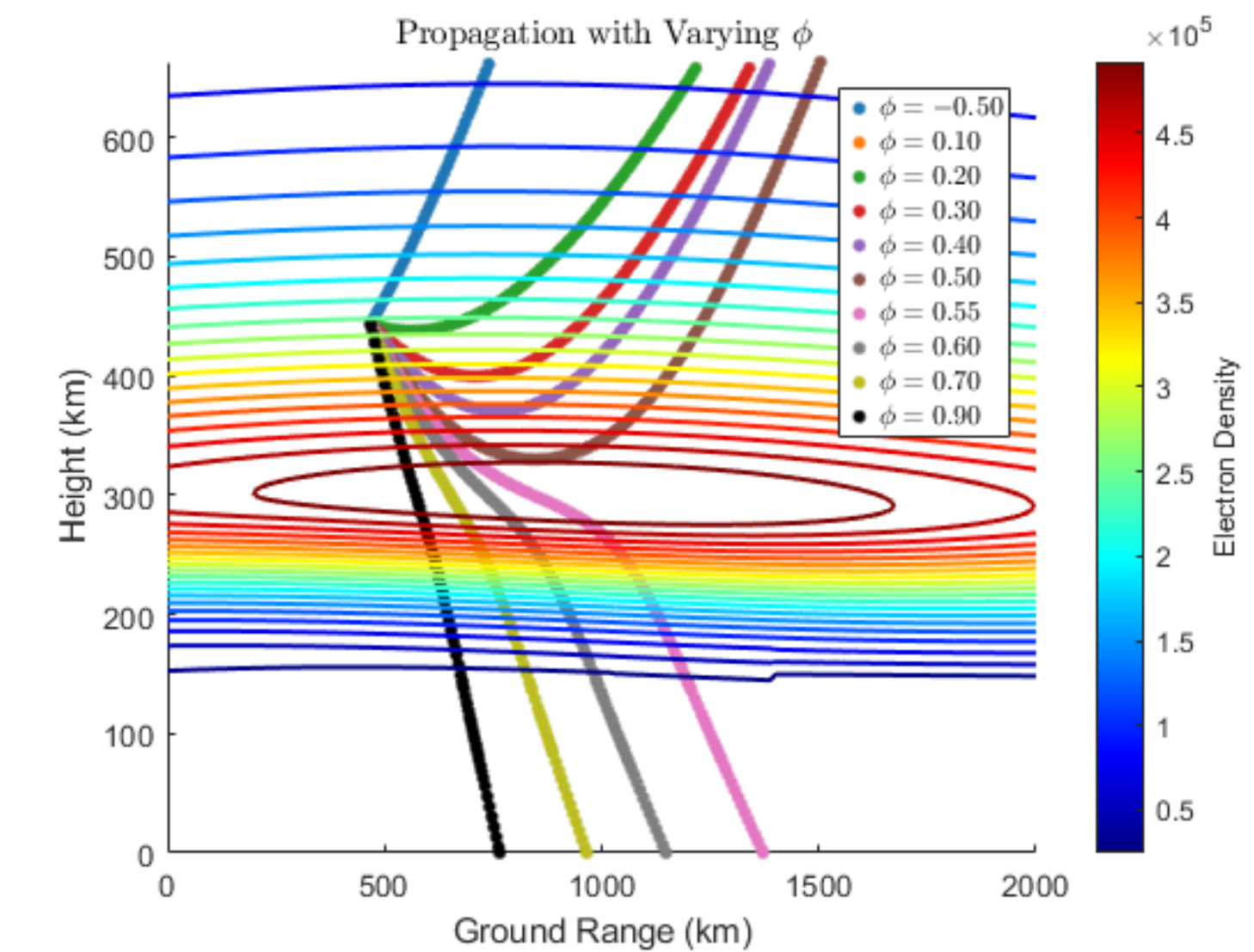
To evaluate potential source heights and compare the different theoretical generation mechanisms of MFB, preliminary ray tracing was done with PHARLAP (Cervera, 2016) This open-source ray tracing software utilizes Fermat's variational principle to minimize the ray path time combined with a Lagrangian approach (rather than Snell's Law). Solutions are in the form of two differential equations for how the functions r and Q change with elevation theta, which can be calculated for each step over the ray path. (Coleman, 1997, 1998) Using the average elevations for individual events will allow for a range of phi values to be traced to the ground to determine if they could be observed by the antenna system, where phi is the launch angle defined by the function

Q(r, theta) = mu sin phi

where mu is the index of refraction mu = (1 - beta N^2)^1/2

N is the electron density in cm^-3, f is the frequency of the wave in MHz, and beta is a constant 8.05 x 10^-3 given by Coleman that can be derived from the dispersion relation. (Chen, 1984)

Two examples of rays traced at nine different phi values are shown to the right, superposed over the electron density contours (cm^-3) generated by IRI. The upper figure rays start around 450 km, well above the densest region, and have a critical angle of refraction between 0.50° and 0.55°. The lower figure rays start around 350 km, just within the densest region, and have a critical angle of refraction between 0.20° and 0.30°. Since hiss propagates at VLF and requires Whistler mode, which requires f < min(fce, fpe) the 3D version of PHARLAP will be needed to include the magnetic field. Another option is to use a different ray tracing software that was designed for VLF propagation to simulate the hiss.



An example of the Sondrestrom ISR electron density composite scan data from Broughton et al. is shown to the left. The upper figure shows the electron density just before substorm onset, and the lower shows that just after onset. The data for these figures is available through Madrigal under Sondrestrom ISR. Some progress has already been made in recreating the profiles shown to the left for one of the simultaneous events in which data is available, but the exact interpolation method used is still unknown. The best fit tried so far has been to generate a mesh grid in python. The electron density error still needs to be included, which is shown in the figures to the left. Additionally, the mesh grid and the electron density grid in PHARLAP will need to be adjusted to match in terms of ground range and height. The electron density measurement error of 2 x 10^10 m^-3 given in the figures to the left will also need to be incorporated into the data set and mesh grid.

The days that have data available will likely be used as case studies. For days that do not have data, it would be best to use a profile from a similar event, around the same time of year. This would still be a much better approximation than what is provided by IRI at high latitudes. Additionally, IRI does not capture the substantial increase to the electron density in certain regions as is the case during a substorm. This can be seen by comparing the color bars of the figures above and to the right: the IRI profile above has a maximum of 5 x 10^5 cm^-3, the ISR profile to the left has a maximum of 2 x 10^11 m^-3.

References

1. Broughton, M. C., J. LaBelle, G. T. Roberg-Clark, M. McCready, and N. L. Bunch (2012), Experimental tests of a topside generation mechanism for auroral medium frequency radio emissions, J. Geophys. Res., 117, A12309, doi:10.1029/2012JA018034.
2. Bunch, N. L., LaBelle, J., Weatherwax, A. T., Hughes, J. M., & Lummerzhelm, D. (2009). Experimental tests of the generation mechanism of auroral medium frequency burst radio emissions. Journal of Geophysical Research: Space Physics, 114(A9).
3. Cervera, M. (2016). Pharlap. Defence Science and Technology Group.
4. Chen, F. F. (1984). Introduction to plasma physics and controlled fusion (Vol. 1, pp. 19-51). New York: Plenum press.
5. Coleman, C. J. (1997). On the simulation of backscatter ionograms. Journal of Atmospheric and Solar-Terrestrial Physics, 59(16), 2089-2099.
6. Coleman, C. J. (1998). A ray tracing formulation and its application to some problems in over-the-horizon radar, Radio Sci., 33(4), 1187-1197, doi:10.1029/98RS01523.
7. Dodge, Y. (2008). The concise encyclopedia of statistics. Springer Science & Business Media.
8. Gjerloev, J. W. (2012). The supermag data processing technique. Journal of Geo-physical Research: Space Physics, 117 (A9).
9. Kletzing, C. A., F. S. Mozer, and R. B. Torbert (1998). Electron temperature and density at high latitude, J. Geophys. Res., 103(A7), 14837-14845, doi:10.1029/98JA00962.
10. LaBelle, J., S. G. Shepherd, and M. L. Trimpi (1997). Observations of auroral medium frequency bursts, J. Geophys. Res., 102(A10), 22221-22231, doi:10.1029/97JA01905.
11. LaBelle, J. (2011). An explanation for the fine structure of MF burst emissions, Geophys. Res. Lett., 38, L03105, doi:10.1029/2010GL046218.
12. Muscietti, L. (1990). Electron beam formation and stability. Solar physics, 130, 201-228.

Contact: tedi.m.godfrey.gr@dartmouth.edu

Acknowledgements: Financial support provided by NSF Grant AGS-1915058 to Dartmouth College and NASA New Hampshire Space Grant 80NSSC20M0051. We gratefully acknowledge the SuperMAG collaborators (https://supermag.jhuapl.edu/info/?page=acknowledgement). Some results shown in this poster were obtained using the HF propagation toolbox, PHARLAP, created by Dr. Manuel Cervera, Defence Science and Technology Group, Australia (manuel.cervera@dsto.defence.gov.au). This toolbox is available by request from its author. Thanks to David McGaw for instrumentation engineering.